Structural Analysis and Optimization of NK_1 Receptor Antagonists through Modulation of Atropisomer Interconversion Properties

Jeffrey S. Albert,* Cyrus Ohnmacht, Peter R. Bernstein, William L. Rumsey, David Aharony, Yun Alelyunas, Daniel J. Russell, William Potts, Scott A. Sherwood, Lihong Shen, Robert F. Dedinas, William E. Palmer, and Keith Russell

CNS Discovery Research, AstraZeneca Pharmaceuticals LP, 1800 Concord Pike, P.O. Box 15437, Wilmington, Delaware 19850-5437, and EST, AstraZeneca Pharmaceuticals LP, Waltham, Massachusetts 02451

Received April 24, 2003

We have previously described a series of antagonists that showed high potency and selectivity for the NK_1 receptor. However, these compounds also had the undesirable property of existing as a mixture of interconverting rotational isomers. Here we show that alteration of the 2-naphthyl substituent can modulate the rate of isomer exchange. Comparisons of the NK_1 receptor affinity for the various conformational forms has facilitated the development of a detailed NK_1 pharmacophore model.

Downloaded via 216.241.254.30 on August 28, 2025 at 17:51:36 (UTC).
See https://pubs.acs.org/sharingguidelines for options on how to legitimately share published articles.

Introduction

The tachykinins are a family of three mammalian neuropeptides: substance P (SP), neurokinin A (NKA), and neurokinin B (NKB). The preferred receptors for these are termed NK_1, NK_2, and NK_3, respectively. The NK_1 receptor is widely distributed in the CNS and peripheral tissue; SP acts as a neurotransmitter or neuromodulatory agent. The NK_1 receptor may be involved in several pathophysiological conditions including asthma, emesis, anxiety, depression, and pain.[1,2] The areas of neurokinin antagonist development have been extensively reviewed.[3−6]

We have described the identification of the orally active, dual NK_1/NK_2 receptor antagonist ZD6021 (**1**).[7,8] In subsequent work, it was found that, for compounds related to **1**, substitutions at the naphthyl 2-position altered the NK_1/NK_2 receptor selectivity. This led to the identification of ZD4974 (**2**) as a potent, orally available, NK_1-selective antagonist.[9]

In compound **2**, the naphthalene 2-methoxy substituent was necessary for NK_1 selectivity; however, it also caused the compound to exist in solution as a mixture of atropisomers (equilibrating conformational isomers). Due to the restricted rotations at the amide and carbonyl−aryl bonds (Figure 1), a total of four atropisomers were evident by high-pressure liquid chromatography (HPLC) and NMR spectroscopy.

Despite its oral potency, progression of **2** as a potential drug would be complicated because of the existence of multiple conformational forms; these could present significant challenges due to potential safety, analytical, and manufacturing concerns.[10,11] To address this, we have analyzed the kinetic properties and structure−activity relationships (SARs) for **2** and for related naphthyl-substituted analogues. These efforts have led to the identification of **3**, which had biological properties similar to those of **2**, but had improved kinetic properties and could be isolated in a single conformational form. In this paper, we describe the structural and biological properties of **3**, and we propose an NK_1 receptor pharmacophore model for its activity.

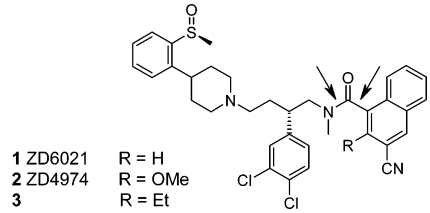

Figure 1. Structures of **1**−**3**. Arrows indicate bonds with restricted rotation.

Chemistry

Compounds **3**−**8** could be accessed from the trisubstituted naphthalene **9**, which was readily available from prior work.[9] Synthetic procedures are illustrated for the preparation of **3**. Selective demethylation of the methyl ether in **9** was carried out using magnesium iodide (Scheme 1).[12] The resulting naphthol **10** was converted to triflate **11**, which was coupled with tributylvinyltin in the presence of lithium chloride, tetrakistriphenylphosphine palladium, and 2,6-di-*tert*-butyl-4-methylphenol to afford **12** in good yield. The vinyl group was reduced using hydrogen in the presence of palladium on carbon to afford **13**. Using trimethylsilyl iodide, the methyl ester of **13** was converted to carboxylic acid **14**. This material was converted to the acid chloride and then reacted with *N*-[(*S*)-2-(3,4-dichlorophenyl)-4-[4-[(*S*)-2-methylsulfinylphenyl]-1-piperidinyl]butyl]-*N*-methylamine[7] to give **3**. Using analogous approaches, **4**−**8** were prepared from **9**.

Results

(a) Influence of the 2-Naphthyl Substituent on Naphthyl−Carbonyl Bond Rotation. For compounds containing the naphthamide group, rotation is restricted at the amide and the naphthyl−carbonyl bonds (Figure 1) due to resonance and steric effects. In such systems, four atropisomers can potentially result since each bond

* To whom correspondence should be addressed at CNS Discovery Research. Phone: (302) 886-4771. Fax: (302) 886-5382. E-mail: jeffrey.albert@astrazeneca.com.

10.1021/jm030197g CCC: $27.50 © 2004 American Chemical Society
Published on Web 12/23/2003

HELSINN EXHIBIT 2045
Azurity Pharmaceuticals, Inc. v. Helsinn Healthcare S.A.
IPR2025-00949

Scheme 1[a]

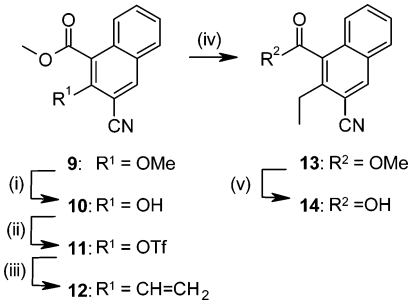

[a] Reagents: (i) Mg, I_2 (73%); (ii) trifluoromethanesulfonic anhydride, triethylamine (97%); (iii) tributylvinyltin, lithium chloride, tetrakis(triphenylphosphine)palladium, and 2,6-di-*tert*-butyl-4-methylphenol (91%); (iv) H_2 (g), 5% palladium on carbon (89%); (v) (TMS)I (95%).

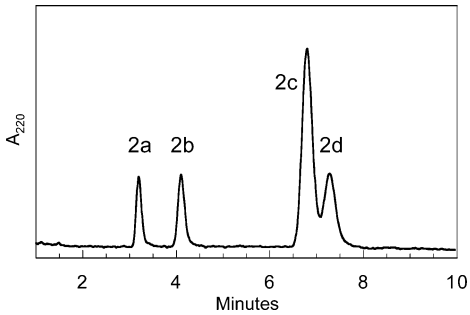

Figure 2. High-pressure liquid chromatogram of **2** showing the resolution of the atropisomeric forms (**2a**−**d**). Conditions: column Phenomonex Luna C18(2) (3 μm, 4.6 × 75 mm), 53% methanol, 47% water (0.1% TFA), 1.5 mL/min, UV detection at 220 nM.

can assume two orientations (s-cis and s-trans for the amide bond, axial-*R* and axial-*S* for the naphthyl−carbonyl bond).[13] For **1** and analogues where R = H (Figure 1), NMR spectra at room temperature were broadened due to the presence of multiple conformational forms. Interconversion between the forms appeared to be relatively rapid since (1) the conformers could not be resolved by HPLC and (2) moderate heating (50−60 °C) caused coalescence of the NMR resonances from the individual conformers.

In such naphthamide systems, it is known that the rate of interconversion is sensitive to the nature of substitution at the naphthamide 2- and 8-positions.[14,15] Introduction of a methoxy group to the naphthyl ring (to afford **2**) substantially increased the bond rotational barrier; four distinct components could be observed by HPLC, shown in Figure 2, and NMR spectroscopy. Samples that were enriched in the major atropisomer of **2** (**2c** in Figure 2) were obtained by preparative HPLC of the atropisomer mixture. Using analytical HPLC, we monitored the reequilibration of the atropisomers and estimated the interconversion half-life to be 2−4 h (pH 7.4, 100 mM phosphate, 37 °C). Because this rate is near the expected biological lifetime of the compound, it would be likely that exposure would occur to all atropisomers even if the compound was administered in a single conformational form. Therefore, it was judged to be unacceptable for further drug development despite its potent and selective activity as an NK_1 receptor antagonist.

Systematic studies of bond rotation rates have been carried out by Clayden for closely related 2-substituted naphthamides.[14,16] These studies indicated that the bond rotation rate was substantially influenced by the nature of the 2-substituent. This prompted us to examine a series of analogues of **2** with the goal of either accelerating bond rotation (to reach the fast exchange regime) or retarding bond rotation (to enable isolation and storage of the active component).

Table 1. Receptor Affinity (pK_B) for Substituted Aryl Sulfoxide Piperidine Analogues of **2**[a]

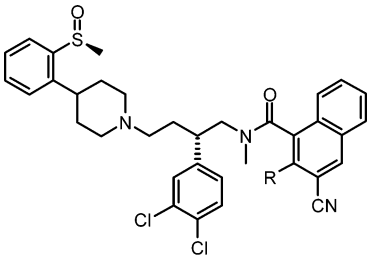

compd	R	NK_1[b]	NK_2[c]
1	H	9.00 ± 0.11	8.30 ± 0.12
2	OMe	9.50 ± 0.11	7.50 ± 0.03
3	Et	9.56 ± 0.04	7.31 ± 0.28
4	Me	9.06 ± 0.27	7.10 ± 0.01
5	$CH_2CH_2CH_3$	7.80 ± 0.46	6.72 ± 0.33
6	$CH_2CH(CH_3)_2$	7.23 ± 0.18	6.35 ± 0.09
7	Ph	7.39 ± 0.30	7.27 ± 0.16

[a] pK_B determinations using rabbit pulmonary artery tissue (n = 2−6). [b] Agonist ASMSP ((Ac-(Arg^6,Sar^9,Met(O$_2$)^{11})SP$_{6-11}$). [c] Agonist BANK (β-Ala^{8}NKA(4−10)).

(b) 2-Substituted Naphthamide Analogues of 2. A series of 2-substituted naphthamide derivatives were investigated to identify potent NK_1 receptor antagonists which minimized complications due to multiple atropisomeric forms. In addition, we sought to find a replacement for the naphthol ether group in **2** to reduce the potential for metabolic liabilities.

As expected from prior studies,[9] the 2-naphthyl-substituted compounds **3**−**7** showed reduced receptor binding affinity for NK_2 in comparison to **1** (Table 1). Additionally, all compounds existed as a mixture of four conformational forms as evidenced by HPLC and NMR. Replacement of the methoxy group of **2** with methyl (**4**) led to slightly reduced affinity at NK_1. Replacement with ethyl (**3**) resulted in a retention of high NK_1 receptor affinity. Replacement with larger groups (**5**−**7**) led to substantially reduced NK_1 receptor affinity. The most potent among these (**3**) was selected for further evaluation in biological and structural studies.

(c) Rate of Atropisomer Interconversion for 3. The four atropisomeric components in the equilibrium mixture of **3** were separated using preparative HPLC in a manner similar to that for **2**. The individual components were designated as **3a**, **3b**, **3c**, and **3d** in order of increasing HPLC retention times (these designations are analogous to those for compounds **2a**, **2b**, **2c**, and **2d** in Figure 2). Atropisomer interconversion was monitored by analytical HPLC starting from each of the isolated isomers in aqueous solution. Results were independent of conditions of pH between 4 and 8 and temperature between 50 and 70 °C. Interconversion occurred predominately between pair **3a**/**3d** and pair **3b**/**3c**. Interconversion among all other atropisomers was minimal under the time scale studied (up to 18 h at 70 °C). The rate for the disappearance and appearance of

Table 2. Antagonist Binding to Human Tachykinin Receptors [K_i (nM)][a]

compd	NK_1[b]	NK_2[c]	NK_3[d]
3	1.24 ± 0.15	37 ± 6	97 ± 11
3a	1.71 ± 0.43	23 ± 3	nd[e]
3b	0.40 ± 0.10	35 ± 4	nd[e]
3c	2.94 ± 0.57	22 ± 6	nd[e]
3d	6.94 ± 0.85	33 ± 3	nd[e]

[a] Human tachykinin receptor expressed in mouse erythroleukemia cells, $n \geq 2$ determinations. [b] Against [^{3}H]SP. [c] Against [^{125}I]NKA. [d] Against [^{125}I]MePheNKB. [e] Not determined.

the corresponding isomer obeyed first-order kinetics and was pH independent between pH 4 and pH 8. The activation energy for atropisomer interconversion was determined to be 24 ± 1 kcal/mol by Arrhenius extrapolation of rate constants obtained at different temperatures. This corresponds to a half-life of about 1.8 days at 37 °C. The observed interconversion rate is consistent with rates seen for related systems.[14,16] Solid samples of **3d** (as the citrate salt) showed no changes in atropisomer distribution upon storage at room temperature for four weeks; this indicated that any reequilibration in the solid state must be very slow. Compared to the expected biological half-life of the compound (discussed below), the extrapolated half-life at 37 °C is slow (1.8 days); hence, **3** was judged to be acceptable for further investigation.

(d) Comparison of Atropisomeric Forms of 3. Human Receptor Binding Affinity. Receptor binding affinity was determined for each of the isolated atropisomers of **3** (Table 2). By keeping the individual atropisomers chilled during the purification and sample preparation, we minimized reequilibration. Prior to initiating studies, we verified that each atropisomer had a purity level of >95%. An exception was for atropisomer **3a**; some batches had a purity level of only >90%.

We found NK_1 receptor binding affinity varied over approximately a 17-fold range from 0.40 nM (**3b**) to 6.94 nM (**3d**). For each, receptor affinity was higher for NK_1 than for NK_2. However, selectivity was weak; NK_1 receptor affinity was greater than NK_2 affinity by only about 5−20-fold. NK_3 receptor affinity was somewhat weaker (K_i = 97 nM) for the equilibrium mixture (**3**); NK_3 receptor affinities for the individual atropisomers were not determined.

(e) Comparison of Atropisomeric Forms of 3. In Vitro Activity. Throughout our tachykinin research program, for compounds in this series, we have continually observed that when receptor binding affinity (to human receptors expressed in mouse erythroleukemia (MEL) cells) is in the nanomolar range, there tends to be a poor correlation between these data and measures of in vivo potency when analyzed in various guinea pig, rabbit, and gerbil assays. We often observed differences of 20−50-fold, or even greater, in animal models among compounds that showed similar, and high, human receptor binding affinity. This occurs despite the high homology among human, guinea pig, rabbit, and gerbil tachykinin receptors. This apparent discrepancy becomes more pronounced for compounds of higher affinity; in these cases the human receptor binding affinity appears to plateau, and greater differences are seen in the in vivo and tissue models. As a consequence of this, and the generally good correlation between potency

Table 3. In Vitro Receptor Activity (pK_B) Using Rabbit Pulmonary Artery[a]

	NK_1			NK_2
compd	pK_B[b]	% inhibition at [antagonist] = 100 nM[d]	% inhibition at [antagonist] = 10 nM[d]	pK_B[e]
3	9.56 ± 0.04	62	nd[c]	7.31 ± 0.28
3a	nd[c]	89	<10	7.11± 0.08
3b	nd[c]	51	nd[c]	7.79 ± 0.21
3c	nd[c]	22	nd[c]	6.83 ± 0.11
3d	nd[c]	98	73	6.25 ± 0.06

[a] pK_B determinations using rabbit pulmonary artery tissue (n = 2−6). [b] Agonist ASMSP, antagonist concentration 1 nM. [c] Not determined. [d] Because these compounds displayed nonpurely competitive antagonism, activity is evaluated by monitoring the magnitude of the maximum tissue relaxation response (control response, ±5%); values are expressed as percent inhibition, which is calculated as 100 − percentage of control response; larger values indicate greater potency.[17] Agonist ASMSP, antagonist concentration 100 nM. [e] Agonist BANK, antagonist concentration 1 μM.

measures in multiple animal models, we base our compound evaluation and SAR analysis on results from animal models and isolated tissue response data rather than binding data to human receptors expressed in mouse erythroleukemia cells.

Pharmacological activity and selectivity were assessed in vitro using pulmonary artery isolated from rabbit (RPA). As noted above, rabbit neurokinin receptors are homologous to human neurokinin receptors. Using RPA, NK_2 receptor potency (pK_B) of the individual atropisomers of **3** (Table 3) varied by about 10-fold; **3b** was the most potent (pK_B = 7.79), while **3d** was the least (pK_B = 6.25). For the NK_1 receptor, **3** induced a suppression of the maximal response to added agonist. Such behavior is often associated with noncompetitive or partially competitive antagonism; in these cases, pK_B cannot be determined. However, the pK_B value of **3** could be estimated using very low antagonist concentration to minimize effects on the maximal relaxation response. To compare the NK_1 receptor antagonist activities among the individual atropisomers (**3a**−**d** at 100 nM), the magnitude of the inhibition of the maximum agonist-mediated tissue relaxation response in the presence of antagonist was calculated in comparison to the agonist-mediated relaxation response in the absence of drug. Greater antagonist activity was indicated by increased percent inhibition (Table 3).[17] Accordingly, NK_1 receptor activity varied in the following rank order: **3d** > **3a** > **3b** > **3c** (affinity for **3a** is likely to be even weaker than indicated because the tested sample contained 10% of the most active compound **3d** as a contaminant). At lower antagonist concentration (10 nM) it was clearly demonstrated that antagonist activity was greater for **3d** than for **3a**.

It is notable that the ranking of activity for compounds **3a**−**d** is different between human receptor binding affinity (Table 2) and RPA receptor antagonist activity (Table 3). As explained above, the apparent inconsistency between the results in these models has been previously observed for structurally related compounds; many have shown similar and high receptor binding affinity in cloned MEL cells although they have quite different activities in functional models.[9] Reasons for this difference have not been thoroughly investigated, but could be due to factors including differences in receptor expression or compound exposure in the

Table 4. Inhibition of ASMSP-Induced Foot-Tapping Response in Gerbil[a]

compd	% inhibition of response	compd	% inhibition of response
3	33 ± 17	**3c**	0.3 ± 0.1
3a	1.4 ± 0.8	**3d**	91 ± 9
3b	13 ± 11		

[a] Determined 6 h after oral dosing of antagonist at 5 umol/kg and initiated by CNS administration of ASMSP (100 pmol); greater values indicate higher compound potency. $n = 4-8$.

models. Because of this apparent discrepancy, we rely on a combination of in vivo and tissue-based models to evaluate compound potency, as explained above.

(f) Comparison of Atropisomeric Forms of 3. In Vivo CNS Activity and Pharmacokinetic Analysis. Central administration of ASMSP to gerbils induces a foot-tapping response which can be attenuated by prior dosing with an orally available CNS-penetrant, NK_1 receptor antagonist. This can provide a convenient way to assess activity of NK_1 receptor antagonists.[18] Gerbils were orally treated with antagonist at 5 μmol/kg 6 h prior to administration of agonist. The CNS activity was then monitored by comparing the degree of foot-tapping response with control animals that were treated with antagonist vehicle only. Among the four atropisomers, **3d** showed the greatest NK_1 receptor antagonism in the foot-tapping model (Table 4); this compound also had the greatest effect in RPA tissue (Table 3).

We note that although **3d** showed the highest potency in the rabbit pulmonary artery tissue functional assay (Table 3) and the highest potency in the gerbil foot-tapping assay (Table 4), it did not show the highest affinity among the four atropisomers to human receptors expressed in MEL cells (Table 2). As explained above, throughout our tachykinin program, compounds in this chemical series tend to show better consistency among rabbit tissue models, guinea pig in vivo models, and gerbil in vivo models than for binding to human receptors expressed in MEL cells. For this reason, we regard the tissue models and in vivo studies (particularly in combination) as a more reliable measure of compound potency than binding to human receptors expressed in MEL cells.

To determine which was the NK_1-preferring atropisomer, we compared the potency of each individual purified component in the rabbit pulmonary tissue functional model and the gerbil foot-tapping model. At the time each experiment was initiated, we confirmed that the atropisomer sample under study was present at a purity of >95% (with the exception of **3a**, which had a purity level of >90%, containing primarily **3d** as the minor, contaminating species). On the basis of the potency results from the rabbit pulmonary tissue functional model and the gerbil foot-tapping model, we assign **3d** as the preferred NK_1 atropisomer.

However, it is possible that the atropisomer distribution could change during the course of the experiments. This is a particular concern for testing in the gerbil foot-tapping model because the atropisomer ratios could potentially be influenced by, for example, the presence of plasma proteins or endogenous rotamases during the long time course of the experiments (up to 6 h). To confirm that the potent activity of **3d** in the gerbil model was indeed due to **3d** alone (and not due to other atropisomers which could potentially have accumulated from interconversion during the experimental time course), we analyzed the atropisomer distribution in gerbil plasma samples. Using identical protocols for the gerbil foot-tapping model, **3d** was orally administered to gerbils ($n = 6$). At times of 1 and 6 h following administration, plasma samples were analyzed by LC–MS to determine the atropisomer distribution. We found that the distribution of **3d** remained consistent at 95 ± 1% from the initial point of dosage, at the 1 h interval, and at the 6 h interval. The distribution of the major contaminating atropisomer (**3c**) also remained constant at about 4.1%. These results confirm that the suppression of the foot-tapping response is due to **3d** and not due to other forms.

Pharmacokinetic analysis indicated that **3** had 37% oral bioavailability with a biological half-life of about 6 h in dog (Table 5). Since the atropisomer interconversion rate (approximately 1.8 days) was about 7-fold slower than the biological elimination rate in dog, it is possible that dosing with the single atropisomer **3d** would result in minimal exposure to the three other atropisomers. Unfortunately, we were unable to analyze the atropisomer distribution of samples from animal studies (in biological matrixes) due to insufficient chromatographic resolution in dog. Pharmacokinetic parameters are summarized in Table 5.

(g) Structural Analysis of 3. The atropisomers of **3** could be individually analyzed by NMR because of the relatively slow interconversion among them. The chemical shifts from the amide *N*-methyl protons of **3a** and **3b** were shifted downfield relative to those of **3c** and **3d** (Table 6). Such a downfield shift is expected when the methyl group is oriented near the carbonyl oxygen; this is possible only in the *cis*-amide configuration. The corresponding effect is observed for the H16 protons; in this case the H16 protons in **3c** and **3d** are shifted downfield relative to those of **3a** and **3b**. Again, this downfield shift is expected in the *trans*-amide configuration due to the proximity of those protons to the amide–carbonyl bond. In this manner, we provisionally assigned *trans*-amide configurations to **3c** and **3d**, and *cis*-amide configurations to **3a** and **3b**.

It is also notable that the chemical shifts for H8 of **3b** and (particularly) **3d** are significantly upfield in comparison to the more typical shifts for H8 in **3a** and **3c**. The upfield shift of the H8 proton in **3d** suggests that it may be located proximal to the shielding region of the dichloroaryl ring. NMR data for H4 are included

Table 5. Pharmcokinetic Analysis of **3** in Dog ($n = 3$)

pharmacokinetic param	result	pharmacokinetic param	result
oral dose (μmol/kg)	10	AUC-PO(0–i) [(ng·h)/mL]	6134 ± 4507
formulation	75% PEG/saline	extrapolated AUC (%)	7 ± 2
C_{max} (ng/mL)	662 ± 438	bioavailability (%)	37.3 ± 6.5
T_{max} (h)	4 ± 1	$t_{1/2}$ (h)	5.9 ± 0.6

Table 6. ^{1}H NMR Chemical Shifts of Selected Resonances in Atropisomers of **3**[a]

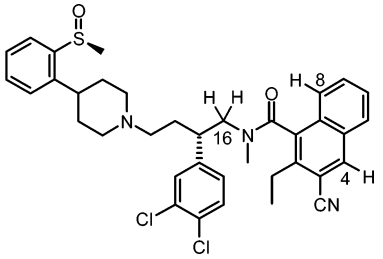

	H4	H8	H16	NMe
3a	8.53	7.67	3.68	3.30
3b	8.49	6.76	3.62	3.32
3c	8.48	7.63	4.88	2.66
3d	8.44	6.19	4.82	2.64

[a] Chemical shifts expressed in parts per million for the midpoint of the spin system, relative to the peak for tetramethylsilane. Spectra were acquired at room temperature in $CDCl_3$.

for reference; the chemical shifts are nearly equivalent for all atropisomers.

NMR had suggested that **3d** (and **3c**) was oriented with a *trans*-amide (vide supra), but the carbonyl−aryl orientation remained uncertain. We assumed that the upfield shifting of the H8 proton resulted from some type of aryl−aryl interaction of the naphthalene with the dichloroaryl ring. Using molecular mechanics modeling, we compared the low-energy conformers for the axial-*R* and axial-*S* carbonyl structures (each with the *trans*-amide). Low-energy conformers with the axial-*S* configuration directed H8 toward the dichloroaryl ring (consistent with NMR data), whereas low-energy conformers with the axial-*R* configuration had H8 directed away from the dichloroaryl ring. On the basis of this, we associated **3d** with *S* stereochemistry of the carbonyl−aryl bond. NMR had also suggested that **3b** contained a *cis*-amide; analogous modeling studies comparing the axial-*R* and axial-*S* carbonyl structures for the *cis*-amide-containing **3b** allowed us to associate **3b** with *S* stereochemistry of the carbonyl−aryl bond. Taken together, we propose the structural assignment for each of the atropisomers as shown in Figure 3. Although these data all refer to studies conducted in $CDCl_3$, similar chemical shift changes were observed for each atropisomer in deuterated methanol and deuterated dimethyl sulfoxide. Unfortunately, we were unable to observe nuclear Overhauser effects between H4 or H8 and the dichloro ring in any of the atropisomers studied.

These structural assignments are further consistent with the kinetic results; as noted above, we observed that the fastest interconversion occurred between pair **3a**/**3d** and pair **3b**/**3c**. Very slow interconversion occurred between all other pairs. According to our structural assignment, the fastest interconversions would be due to the *simultaneous* inversion of both the amide bond and the carbonyl−aryl bond. Independent rotation of either the amide or carbonyl−aryl bonds (leading to direct interconversion between pair **3d**/**3b**, **3b**/**3a**, **3a**/**3c**, or **3c**/**3d**) would be much slower according to these observations.

This type of simultaneous, paired interconversion has been observed for similar naphthamide-containing systems.[16] In these cases, it is understood that inversion of the carbonyl−aryl bond causes steric clashes with the amide which are relieved by distortion (and concomitant rotation) of the amide bond. Amide rotation would similarly be facilitated by distortion/rotation of the carbonyl−aryl bond. Such interdependence is referred to as geared rotation.[19]

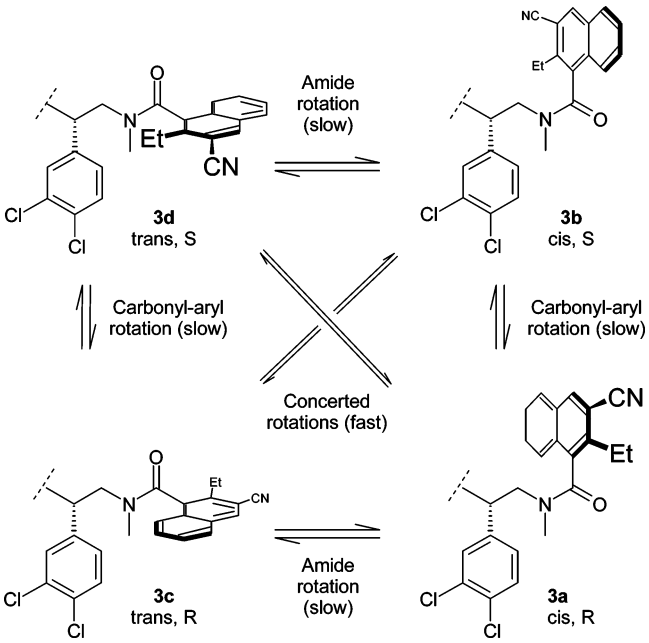

Figure 3. Structural assignments for atropisomers **3a**−**d**.

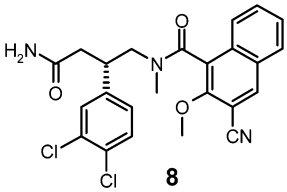

Figure 4. Structure of **8**.

Unfortunately, crystals of **3d** were unsuitable for crystallographic analysis. However, useful crystals were obtained for the truncated analogue **8** in which the piperidine group was removed (Figure 4). In solution, **8** also exists as a mixture of atropisomers, but can be easily crystallized and isolated in a single form. NMR spectral properties of the crystallized form of **8** are similar to those of **3d**; the H8 and the NMe signals are shifted upfield (δ 6.35 and 2.62, respectively). As for **3d**, these results suggest a conformation involving the *trans*-amide and an (*S*)-carbonyl−aryl bond. Furthermore, **8** does show NK_1 receptor antagonist activity.[20] For **8**, the *trans*-amide, (*S*)-carbonyl amide assignment was confirmed by crystallographic analysis (Figure 5). In addition, the crystal structure shows that the naphthyl and dichloroaryl rings of **8** are positioned to allow an edge-to-face aryl−aryl stacking interaction as originally proposed for **3d** on the basis of NMR data. The plane of the naphthalene is nearly orthogonal to the plane of the dichloroaryl ring, and the naphthalene H8 is located 3.4 Å from the dichloroaryl ring centroid (2.9 Å from the nearest carbon of the dichloroaryl ring).

(h) Development of a Pharmacophore Model for 3d. Evidence from NMR is consistent with a structural model for **3d** where the dichloroaryl and naphthalene

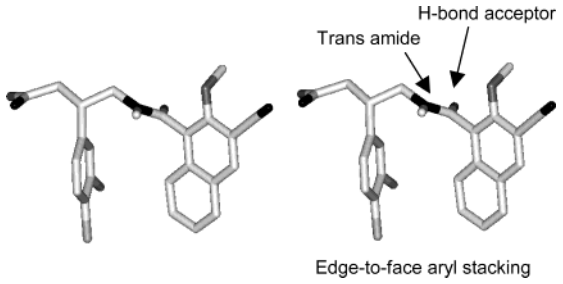

Figure 5. Crystal structure of **8** (relaxed-eye stereo representation with hydrogens omitted for clarity).

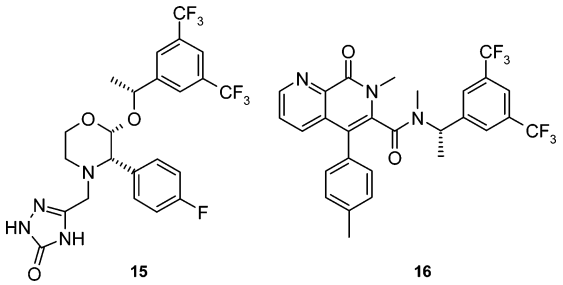

Figure 6. Potent, selective NK_1 receptor antagonists **15**[34] and **16**.[29]

assume orientations analogous to those seen in the crystal structure of **8**. These results suggest a binding model involving an edge-to-face stacking interaction between the dichloroaryl and the naphthalene rings.

An NK_1 receptor pharmacophore model involving stacked aryl rings has been implicated in numerous structural studies on the basis of crystallographic and solution experiments[21−30] as well as modeling.[31−33] Additionally, many NK_1 pharmacophore models have suggested the requirement for a hydrogen bond acceptor in the vicinity of the aryl stacking region. Consistent with this, we found that NK_1 receptor activity was lost for the analogue containing the reverse amide, or replacement of the amide with a sulfonamide (data not shown). Another example where a hydrogen-bonding group seems necessary can be found in the development of MK-869[21,34] (**15**; Figure 6). This is a potent and selective NK_1 receptor antagonist which showed antidepressant activity in clinical evaluation.[35] The design of this compound included a ketal oxygen to serve as a key hydrogen bond acceptor. By building upon this model, a subsequent family of compounds was developed which contained a highly preorganized spirocyclic core and which maintained a ketal oxygen as a critical hydrogen-bonding acceptor.[36]

Computational evaluation of the pharmacophore model was carried out by analysis of a set of compounds related to **3** (which spanned a wide range of receptor binding affinity) along with all the structural information known to us. The software program CATALYST[37] was used to generate and rank possible pharmacophore models. The appropriateness of a given model was assessed by (1) correlations between predicted and measured affinity of the various antagonists and (2) the involvement of an aryl−aryl stacking interaction and hydrogen bond acceptor group.

Our proposed model for **3d** shares key features with models for chemically diverse NK_1 receptor antagonists from Merck[21] (**15**) and Takeda[29] (**16**), shown in Figure 6. Structural studies of compounds related to **15** and **16** suggest that the aryl rings may adopt either an edge-to-face or face-to-face interaction. Our results tend to favor an edge-to-face alignment of the aryl rings. Figure 7 shows the predicted conformations of **3d** along with the reference compounds **15** and **16** when fit using our optimized pharmacophore model. This overlay suggests that each compound can adopt an edge-to-face aryl stacking interaction, and each contains a group which could serve as a hydrogen bond acceptor (ketal oxygen for **15** and amide carbonyl for **16**).

In summary, our prior studies had identified **2** as a potent, orally available NK_1 receptor antagonist but which had the undesirable structural property of existing as a mixture of interconverting atropisomers.[9] By altering the substitution at the 2-position of the naphthalene, it was possible to slow the rate of exchange while improving the NK_1 receptor affinity. For the resulting compound (**3**), the individual atropisomers were separated and individually analyzed. Structural analysis of the most potent atropisomer (**3d**) is consistent with an NK_1 receptor binding model that involves an edge-to-face stacking interaction between the dichloroaryl and naphthalene rings, with the naphthalene amide carbonyl serving as a hydrogen bond acceptor. This model is consistent with models for other chemically diverse, high-affinity NK_1 receptor antagonists.

Experimental Section

Biological Studies. The cloning, heterologous expression, and scale-up growth of MEL cells transfected with the NK_1, NK_2, or NK_3 receptor were conducted as previously described for the human NK_2 receptor.[38−41] The human NK_1 receptor was identical to that reported previously,[42,43] whereas the human NK_3 receptor differed from the genomic sequence at AA439 (Cys vs Phe).[44,45] Ligand binding assays were conducted with [^{3}H]SP (for NK_1), [^{3}H]NKA (for NK_2), and [^{125}I]MePheNKB (for NK_3). Cloning of NK_1, NK_2, and NK_3 receptors was conducted as published.[46] Isolated tissue responses (pK_B) and pulmonary mechanics studies were carried out as previously described.[8] For pK_B determinations, different antagonist concentrations were used according to the affinity of the compound under study; concentrations ranged from 10 nM (for the highest affinity antagonists) to 10 μM (for lower affinity antagonists). In the gerbil foot tap model, gerbils were orally treated with antagonist at 5 mmol/kg 6 h prior to administration of ASMSP agonist (100 pmol). The CNS potency was then monitored by comparing the degree of foot tapping response with control animals that were treated with antagonist vehicle only.[18]

Bioavailability Analysis. Compounds were administered to dog ($n = 3$) at 1−10 μmol/kg by iv bolus injection or at 10−100 μmol/kg orally as a solution in 75% polyethylene glycol 400 in normal saline. Blood samples were taken via surgically implanted cannula or by venipuncture over a 24 h period, and plasma was analyzed for unchanged compound by high-pressure liquid chromatography−mass spectroscopy (LC−MS).

Kinetic Analysis. Solutions of each isolated atropisomer (at approximately 1.4 uM) were incubated in 10 mM buffer solution in the presence of 20% 2-methoxyethanol. The buffer solution was prepared using sodium phosphate or sodium acetate with ionic strength adjusted to 100 mM using sodium periodate. The solutions were incubated in an HPLC autosampler holder connected to an external circulator for temperature control, and the reequilibration process was monitored periodically by HPLC at 50, 60, and 70 °C.

Molecular Modeling. For the structural analysis of **3b** and **3d**, molecular mechanics computations were performed in vacuo, using the AESOP[47] force field and the in-house molecular graphics program ENIGMA.[48] Evaluation of the pharmacophore model was carried out by analysis of a set of compounds related to **3** (and covering a wide range of receptor

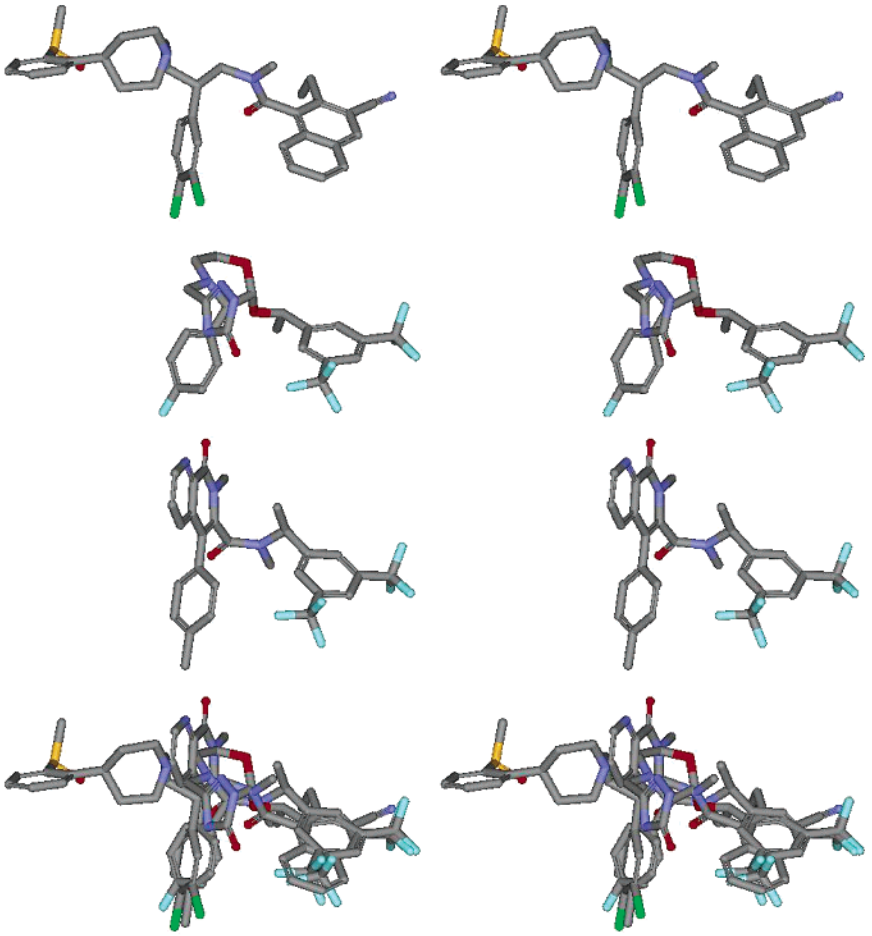

Figure 7. Structures according to the predicted pharmacophore model, from the top **3d**, **15**, and **16**. At the bottom is an overlay of the above three in the same orientation (relaxed-eye stereoview with hydrogens omitted for clarity).

binding affinity) along with all the structural information known to us. Using the software program CATALYST,[37] various potential pharmacophore models were generated that were consistent with the binding affinity results (corresponding to correlations between predicted and measured affinity of the various antagonists). The pharmacophore models were inspected visually and selected for further analysis on the basis of similarity to reported crystal structures and literature pharmacophore models. No single pharmacophore model identified by the program contained all the features implicated in the literature as important for biological activity. However, two pharmacophore models were generated that did contain many of the key features implicated; these were then merged in CATALYST.

Chemistry. ^{1}H NMR spectra were obtained at 300 MHz using a Bruker DPX 300 spectrometer in $CDCl_3$ and were referenced to TMS unless otherwise noted. Mass spectral data were obtained on a Micromass QTOF mass spectrometer. Silica gel chromatography was performed with ICN silica 32-63, 60 Å. Thin-layer chromatography was done on silica gel 60 F-254 (0.25 mm thickness) plates, and visualization was accomplished with UV light. Elemental analyses (C, H, N) were performed on an Exeter Analytical CE-440 elemental analyzer, and all compounds are within 0.4% of theory. All materials were obtained commercially and used without further purification. For compounds containing derivatives of 2-substituted 1-naphthoic acids, ^{1}H NMR spectra and HPLC chromatograms are complex because these compounds exist as a mixture of slow atropisomers. In these cases, ^{1}H NMR integrations are not given.

Methyl 3-Cyano-2-hydroxy-1-naphthoate (10). On the basis of procedures described by Hauser et al.,[12] a flame-dried 250 mL three-neck flask was charged with magnesium metal (2.42 g, 99.5 mmol). After the flask was cooled to room temperature, diethyl ether (80 mL), benzene (30 mL), and iodine (12.62 g, 49.7 mmol) were added. The reaction mixture was heated under reflux for 2 h, and the iodine color dissipated. After being cooled to room temperature, this solution was transferred to methyl 3-cyano-2-methoxy-1-naphthoate[9] (**9**) (10 g, 41.4 mmol) in benzene (30 mL) via syringe. The flask was washed with benzene (15 mL), and a yellow precipitate formed during the addition. The reaction mixture was heated under reflux for 1 h. HCl (1 N) and ethyl acetate were added, and the aqueous layer was extracted with ethyl acetate. The combined organic layers were washed with saturated $Na_2S_2O_4$, NaCl, and water, dried over $MgSO_4$, filtered, and concentrated. The crude product was purified by flash chromatography eluting with dichloromethane (DCM) to afford the product (6.88 g, 73% yield) as a yellow solid: ^{1}H NMR δ 12.82 (s, 1 H), 8.81−8.78 (d, 1 H), 8.32 (s, 1 H), 7.83−7.82 (d, 1 H), 7.70 (t, 1 H), 7.50 (t, 1 H), 4.16 (s, 3 H); MS (negative ion mode) *m/e* 225.92 (M − 1).

Methyl 3-Cyano-2-trifluoromethanesulfonyloxy-1-naphthoate (11). To a solution of **10** (6.24 g, 27.5 mmol) in DCM (140 mL) was added triethylamine (4.21 mL, 30.2 mmol) followed by trifluoromethanesulfonic anhydride (5.05 mL, 30.2 mmol) at 0 °C. The reaction mixture was stirred at room temperature for 30 min. Saturated $NaHCO_3$ was added, and the aqueous layer was extracted with DCM. The combined organic extracts were dried over $MgSO_4$, filtered, and concentrated. The crude product was purified by chromatography (eluting with DCM) to give the product (9.6 g, 97% yield) as a yellow oil: ^{1}H NMR δ 8.44 (s, 1 H), 8.29−8.04 (d, 1 H), 7.01−7.98 (d, 1 H), 7.84 (m, 2 H), 4.10 (s, 3 H).

Methyl 3-Cyano-2-vinyl-1-naphthoate (12). A stirred solution of **11** (10.0 g, 27.8 mmol), tributylvinyltin (8.95 mL, 30.6 mmol), lithium chloride (3.50 g, 83.4 mmol), tetrakis(triphenylphosphine)palladium (0.650 g, 0.556 mmol), and a

few crystals of 2,6-di-*tert*-butyl-4-methylphenol in dioxane (125 mL) was heated to reflux for 3 h. To the cooled mixture was added saturated potassium fluoride solution (150 mL), and the mixture was stirred at room temperature for 0.5 h. This was diluted with ethyl acetate and filtered through Celite. The filtrate was washed with water and saturated sodium chloride, dried over $MgSO_4$, filtered, concentrated, and purified by chromatography (eluting with hexane and 5% ethyl acetate/hexane) to give the product (5.98 g, 91%) as a white solid: ^{1}H NMR δ 8.31 (s, 1 H), 7.90 (d, 1 H), 7.82 (d, 1 H), 7.75−7.59 (m, 2 H), 7.07−6.97 (m, 1 H), 5.87 (d, 1 H), 5.73 (d, 1 H), 4.01 (s, 3 H); MS *m/e* 238 (M + 1).

Methyl 3-Cyano-2-ethyl-1-naphthoate (13). To a solution of **12** (5.98 g, 25.2 mmol) in ethanol (500 mL) was added 5% palladium on carbon (1.5 g); the mixture was shaken under hydrogen (50 psi) overnight. The mixture was filtered through Celite and then concentrated to give the product (5.39 g, 89%) as a light yellow solid: ^{1}H NMR δ 8.28 (s, 1 H), 7.88 (d, 1 H), 7.74 (d, 1 H), 7.67−7.50 (m, 2 H), 4.07 (s, 3 H), 2.96 (q, 2 H), 1.37 (t, 3 H); MS *m/e* 240 (M + 1).

3-Cyano-2-ethyl-1-naphthoic Acid (14). A mixture of **13** (4.87 g, 20.4 mmol) in trimethylsilyl iodide (10 g) was heated at 70−75 °C for 24 h. To the cooled solution was added 1 N HCl, and the mixture was extracted two times with ethyl acetate. The combined organic layers were dried over $MgSO_4$, filtered, and concentrated. The crude product was purified by chromatography (eluting with DCM and then 5% methanol/DCM with 1% acetic acid) to give the product (4.35 g, 95%) as a yellow solid: ^{1}H NMR (DMSO-d_6) δ 14.03 (s, 1 H), 8.69 (s, 1 H), 8.11 (d, 1 H), 7.89−7.77 (m, 2 H), 7.69 (t, 1 H), 2.91 (q, 2 H), 1.29 (t, 3 H); MS *m/e* 224 (M + 1).

***N*-[(*S*)-2-(3,4-Dichlorophenyl)-4-[4-[(*S*)-2-methylsulfinylphenyl]-1-piperidinyl]butyl]-*N*-methyl-3-cyano-2-ethyl-1-naphthamide Citrate (3).** To a solution of **14** (0.14 g, 0.62 mmol) in DCM (5 mL) were added oxalyl chloride (0.07 mL, 0.78 mmol) and a catalytic amount of *N*,*N*′-dimethylformamide. After 2 h, the resulting acid chloride solution was concentrated under reduced pressure and then redissolved in DCM (3 mL). To this solution were added triethylamine (0.14 mL, 1.0 mmol) and *N*-[(*S*)-2-(3,4-dichlorophenyl)-4-[4-[(*S*)-2-methylsulfinylphenyl]-1-piperidinyl]butyl]-*N*-methylamine[9] (262 mg, 0.578 mmol), and the resulting mixture was stirred overnight. The mixture was diluted with DCM, washed with saturated sodium bicarbonate, then dried with $MgSO_4$, filtered, concentrated, and purified by chromatography (eluting with 1%, 2%, and 3% methanol/DCM) to give the product (0.286 g, 75%). After the mass of free base was determined, the material was dissolved in methanol, and 1 equiv of citric acid (81.7 mg, 0.42 mmol) was added. The mixture was concentrated to afford the product as a white powder: ^{1}H NMR δ 8.31−8.19 (m), 7.99−7.82 (m), 7.57−7.31 (m), 7.14−7.11 (d), 7.00−6.98 (m), 6.80 (d), 6.53−6.50 (m), 4.60 (t), 4.38 (t), 3.69−3.49 (m), 3.32−2.55 (m), 2.37−1.61 (m), 1.39−1.10 (m); MS *m/e* 660.32 (M + 1). Anal. Calcd for $C_{37}H_{39}Cl_2N_3O_2S{\cdot}C_6H_8O_7{\cdot}1.70H_2O$: C, 58.46; H, 5.75; N, 4.76. Found: C, 58.51; H, 5.63; N, 4.58.

Methyl 3-Cyano-2-methyl-1-naphthoate (17). A stirred solution of **11** (0.28 g, 0.779 mmol), K_3PO_4 (0.33 g, 1.55 mmol), methylboronic acid (0.096 g, 1.55 mmol), and (1,1′-bis(diphenylphosphino)ferrocene)dichloropalladium(II) ethyl dichloride (64 mg, 0.078 mmol) in tetrahydrofuran (8 mL) was heated at 66 °C for 4.5 h. Saturated aqueous $NaHCO_3$ was added, and the mixture was extracted three times with ethyl acetate. The combined organic layers were dried over $MgSO_4$, filtered, and concentrated. The crude product was purified by chromatography (eluting with 5% and then 8% ethyl acetate/hexane) to give the product (0.139 g, 79% yield) as a white solid: ^{1}H NMR δ 8.28 (s, 1 H), 7.88 (d, 1 H), 7.77 (d, 1 H), 7.67 (t, 1 H), 7.55 (t, 1 H), 4.08 (s, 3 H), 2.66 (s, 3 H); MS *m/e* 226 (M + 1).

3-Cyano-2-methyl-1-naphthoic Acid (18). A solution of **17** (0.139 g, 0.617 mmol) in tetrahydrofuran (7.55 mL) and water (3 mL) was treated with a solution of NaOH (1.3 mL, 1 N). Methanol (0.5 mL) was added, and the mixture was stirred under reflux for 27 h. The mixture was concentrated, treated with additional water, and extracted with DCM. The aqueous layer was acidified with 1 N HCl and extracted with ethyl acetate. The extracts were dried and filtered, and the solvent was removed to afford the product (0.10 g, 77% yield) as a white solid: ^{1}H NMR (300 MHz, DMSO-d_6) δ 14.02 (s, 1 H), 8.67 (s, 1H), 8.08 (d, 1 H), 7.87−7.62 (m, 3 H), 2.59 (s, 3 H); MS (negative ion mode) *m/e* 210 (M − 1).

***N*-[(*S*)-2-(3,4-Dichlorophenyl)-4-[4-[(*S*)-2-methylsulfinylphenyl]-1-piperidinyl]butyl]-*N*-methyl-3-cyano-2-methyl-1-naphthamide Citrate (4).** To a solution of **18** (0.10 g, 0.47 mmol) in DCM (5 mL) were added oxalyl chloride (0.052 mL, 0.59 mmol) and a catalytic amount of *N*,*N*′-dimethylformamide. After 2 h, the resulting acid chloride solution was concentrated under reduced pressure and then redissolved in DCM (1.5 mL). To this solution were added triethylamine (0.104 mL, 0.746 mmol) and *N*-[(*S*)-2-(3,4-dichlorophenyl)-4-[4-[(*S*)-2-methylsulfinylphenyl]-1-piperidinyl]butyl]-*N*-methylamine[9] (0.200 g, 0.44 mmol), and the resulting mixture was stirred overnight. The mixture was diluted with DCM, washed with saturated sodium bicarbonate, then dried with $MgSO_4$, filtered, concentrated, and purified by chromatography (eluting with 1% and then 2% methanol in DCM) to give the product (0.13 g, 42%). After the mass of free base was determined, the material was dissolved in methanol, and 1 equiv of citric acid (38 mg, 0.198 mmol) was added. The mixture was concentrated to afford the product as a light yellow powder: ^{1}H NMR δ 8.23−8.17 (m), 8.01−7.96 (m), 7.84−7.80 (m), 7.62−7.29 (m), 7.10 (d), 6.96 (d), 6.79 (d), 6.50 (d), 4.60−4.52 (m), 4.19−4.11 (m), 3.85−3.79 (m), 3.56−3.50 (m), 3.34−3.15 (m), 3.04−2.88 (m), 2.74−2.53 (m), 2.32−1.60 (m); MS *m/e* 646 (M + 1). Anal. Calcd for $C_{36}H_{37}Cl_2N_3O_2S{\cdot}C_6H_8O_7{\cdot}1.3H_2O$: C, 58.51; H, 5.56; N, 4.87. Found: C, 58.50; H, 5.46; N, 4.82.

Methyl 3-Cyano-2-propyl-1-naphthoate (19). To a stirred solution of **9** (0.300 g, 1.24 mmol) in tetrahydrofuran (6 mL) was added propylmagnesium chloride (2.0 M in ethyl ether, 0.46 mL, 0.92 mmol), and the mixture was stirred at room temperature for 22 h. The reaction was treated with water and DCM, the layers were separated, and the aqueous layer was extracted with three more portions of DCM. The combined organic extracts were dried (Na_2SO_4) and filtered, and the solvent was removed under reduced pressure to yield the product (0.226 g, 72% based on ester): ^{1}H NMR δ 8.28 (s, 1H), 7.88 (d, 1H), 7.76 (d, 1H), 7.67 (m, 1H), 7.58 (t, 1H), 4.07 (s, 3H), 2.91 (m, 2H), 1.77 (m, 2H), 1.05 (t, 3H).

3-Cyano-2-propyl-1-naphthoic Acid (20). A mixture of **19** (0.227 g, 0.91 mmol) and pyridine hydrochloride (2.27 g, 19.6 mmol) was heated at 180 °C for 45 min. After being cooled to room temperature, the solidified mass was treated with water and DCM, the layers were separated, and the aqueous layer was extracted with three additional portions of DCM. The combined organic extracts were dried (Na_2SO_4) and filtered, and the solvent was removed under reduced pressure to yield the product (0.193 g, 89%) as a white solid: ^{1}H NMR δ 8.33 (s, 1H), 8.02 (d, 1H), 7.92 (d, 1H), 7.73 (t, 1H), 7.62 (t, 1H), 3.06 (m, 2H), 1.85 (m, 2H), 1.10 (t, 3H).

***N*-[(*S*)-2-(3,4-Dichlorophenyl)-4-[4-[(*S*)-2-methylsulfinylphenyl]-1-piperidinyl]butyl]-*N*-methyl-3-cyano-2-propyl-1-naphthamide Citrate (5).** To a solution of **20** (0.193 g, 0.81 mmol) in DCM (3 mL) were added oxalyl chloride (0.088 mL, 1.01 mmol) and *N*,*N*′-dimethylformamide (1 drop). After being stirred at room temperature overnight, the resulting acid chloride solution was concentrated under reduced pressure and then redissolved in DCM (3 mL). This solution was added dropwise to a cooled (0 °C) stirred mixture of triethylamine (0.112 mL, 0.81 mmol) and *N*-[(*S*)-2-(3,4-dichlorophenyl)-4-[4-[(*S*)-2-methylsulfinylphenyl]-1-piperidinyl]butyl]-*N*-methylamine[9] (366 mg, 0.81 mmol) in DCM (3 mL), and the resulting mixture was stirred overnight at 0 °C. The reaction mixture was concentrated and purified by flash chromatography (eluting with 2% methanol/DCM) to afford the product (0.398 g, 73%) as a white solid. The material was dissolved in methanol, and 1 equiv of citric acid (113 mg, 0.59 mmol) was added. The mixture was concentrated to afford the product as a white powder: ^{1}H NMR (DMSO-d_6) δ 8.59 (m) 8.08−7.34 (m), 7.10 (m), 6.90 (d), 6.82 (d), 6.35 (d), 4.59 (t), 4.35 (t), 3.66 (dd), 3.51−

3.17 (m) 2.89−2.48 (m), 2.10−1.40 (m), 0.97 (t) 0.76 (t); MS *m/e* 674 (M + 1). Anal. Calcd for $C_{38}H_{41}Cl_2N_3O_2S{\cdot}C_6H_8O_7{\cdot}1.70H_2O$: C, 58.89; H, 5.89; N, 4.68. Found: C, 58.63; H, 5.54; N, 4.86.

Methyl 3-Cyano-2-isobutyl-1-naphthoate (21). A stirred solution of **11** (0.78 g, 2.17 mmol), K_3PO_4 (0.92 g, 4.33 mmol), isobutylboronic acid (0.44 g, 4.33 mmol), and (1,1′-bis(diphenylphosphino)ferrocene)dichloropalladium(II) ethyl dichloride (0.18 g, 0.22 mmol) in tetrahydrofuran (21 mL) was heated at 66 °C for 17 h. Saturated aqueous $NaHCO_3$ was added, and the mixture was extracted three times with ethyl acetate. The combined organic layers were dried over $MgSO_4$, filtered, and concentrated. The crude product was purified by chromatography (eluting with 5% and then 8% ethyl acetate/hexane) to give a white solid as a mixture (0.36 g) of desired product and methyl 3-cyano-1-naphthoate. This mixture was separated by selective basic hydrolysis as follows. A solution of the above mixture (0.36 g) in tetrahydrofuran (23 mL) and water (9 mL) was treated with a solution of NaOH (4.3 mL, 1 N). Methanol (0.5 mL) was added, and the mixture was stirred at room temperature for 1 h. Under these conditions, only methyl 3-cyano-1-naphthoate was converted to the corresponding carboxylic acid, and the remaining methyl 3-cyano-2-isobutyl-1-naphthoate could be easily separated. The mixture was concentrated, treated with additional water, and extracted with DCM. The extracts were dried and filtered, and the solvent was removed to afford the product (0.17 g, 29% yield) as a colorless oil: ^{1}H NMR δ 8.28 (s, 1 H), 7.88 (d, 1H), 7.73 (d, 1 H), 7.66 (t, 1 H), 7.57 (t, 1 H), 4.06 (s, 3 H), 2.89 (d, 2 H), 2.12 (m, 1 H), 0.97 (d, 6 H).

3-Cyano-2-isobutyl-1-naphthoic Acid (22). A mixture of **21** (0.17 g, 0.64 mmol) and trimethylsilyl iodide (5 g) was heated at 70−75 °C for 21 h. HCl (1 N) was added, and the mixture was extracted three times with ethyl acetate. The combined organic layers were dried over $MgSO_4$, filtered, and concentrated. The crude product was purified by chromatography (eluting with DCM and then 5% methanol/DCM with 1% acetic acid) to give the product (0.145 g, 89% yield) as a yellow solid: ^{1}H NMR (DMSO-d_6) δ 14.03 (s, 1 H), 8.69 (s, 1 H), 8.10 (d, 1 H), 7.88−7.72 (m, 2 H), 7.68 (t, 1 H), 2.86 (d, 2 H), 2.08 (m, 1 H), 0.93 (d, 6 H); MS (negative ion mode) *m/e* 252 (M − 1).

***N*-[(*S*)-2-(3,4-Dichlorophenyl)-4-[4-[(*S*)-2-methylsulfinylphenyl]-1-piperidinyl]butyl]-*N*-methyl-3-cyano-2-isobutyl-1-naphthamide Citrate (6).** To a solution of **22** (0.145 g, 0.57 mmol) in DCM (3 mL) were added oxalyl chloride (0.06 mL, 0.71 mmol) and a catalytic amount of *N*,*N*′-dimethylformamide. After 2 h, the resulting acid chloride solution was concentrated under reduced pressure and then redissolved in DCM (3 mL). To this solution were added triethylamine (0.126 mL, 0.90 mmol) and *N*-[(*S*)-2-(3,4-dichlorophenyl)-4-[4-[(*S*)-2-methylsulfinylphenyl]-1-piperidinyl]butyl]-*N*-methylamine (0.24 g, 0.53 mmol),[9] and the resulting mixture was stirred overnight. The mixture was diluted with DCM, washed with saturated sodium bicarbonate, then dried with $MgSO_4$, filtered, concentrated, and purified by chromatography (eluting with 1% and then 2% methanol/DCM) to give the product (0.11 g, 28% yield). After the mass of free base was determined, the material was dissolved in methanol, and 1 equiv of citric acid (27.9 mg, 0.145 mmol) was added. The mixture was concentrated to afford the product as a light yellow powder: ^{1}H NMR δ 8.30−8.19 (m), 8.01−7.98 (m), 7.82−7.80 (m), 7.61−7.32 (m), 7.10 (d), 6.89 (d), 6.72 (d), 6.43−6.40 (m), 4.71 (t), 4.07 (dd), 3.78 (dd), 3.56−3.25 (m), 3.04−1.78 (m), 1.04−0.84 (m); MS *m/e* 688 (M + 1). Anal. Calcd for $C_{39}H_{43}Cl_2N_3O_2S{\cdot}1.55C_6H_8O_7{\cdot}0.1H_2O$: C, 58.70; H, 5.67; N, 4.25. Found: C, 58.45; H, 5.48; N, 4.43.

Methyl 3-Cyano-2-phenyl-1-naphthoate (23). A stirred solution of **11** (0.100 g, 0.28 mmol), K_3PO_4 (0.118 g, 0.56 mmol), phenylboronic acid (0.136 g, 1.12 mmol), (1,1′-bis(diphenylphosphino)ferrocene)dichloropalladium(II) ethyl chloride (0.023 g, 0.028 mmol), and tetrahydrofuran (8 mL) was heated under reflux for 1 h and then stirred at room temperature overnight. The reaction mixture was diluted with ethyl acetate and poured onto saturated $NaHCO_3$ (20 mL); the ethyl acetate layer was collected, washed with brine, dried (Na_2SO_4), and filtered and the solvent removed under reduced pressure. The resulting brown solid was purified by flash chromatography (eluting with DCM) to yield the title compound (0.072 g, 90%) as a white solid: ^{1}H NMR δ 8.41 (s, 1H), 7.96 (t, 2H), 7.70 (m, 2H), 7.46 (m, 5H), 3.64 (s, 3H).

3-Cyano-2-phenyl-1-naphthoic Acid (24). A solution of **23** (0.072 g, 0.25 mmol), trimethylsilyl iodide (0.46 g, 2.29 mmol), and 3 mL of chloroform was stirred at room temperature overnight, heated under reflux for 5 h, concentrated to half the original volume, and then stirred at room temperature overnight. The red-brown reaction mixture was diluted with ethyl acetate and treated with 1 N HCl (5 mL). The ethyl acetate layer was then washed successively with saturated $Na_2S_2O_3$ and brine, dried ($MgSO_4$), and filtered and the solvent removed under reduced pressure to yield the impure product as a light tan solid (0.098 g): ^{1}H NMR (DMSO-d_6) δ 13.68 (br s, 1H), 8.81 (s, 1H), 8.28 (d, 1H), 7.86 (m, 3H), 7.51 (m, 5H).

***N*-[(*S*)-2-(3,4-Dichlorophenyl)-4-[4-[(*S*)-2-methylsulfinylphenyl]-1-piperidinyl]butyl]-*N*-methyl-3-cyano-2-phenyl-1-naphthamide Citrate (7).** To a solution of **24** (0.068 g, 0.25 mmol) in DCM (2 mL) were added oxalyl chloride (0.036 mL, 0.42 mmol) and *N*,*N*′-dimethylformamide (5 μL). After 1.5 h, the resulting acid chloride solution was concentrated under reduced pressure and then redissolved in DCM (2 mL). To this solution were added triethylamine (0.097 mL, 0.70 mmol) and *N*-[(*S*)-2-(3,4-dichlorophenyl)-4-[4-[(*S*)-2-methylsulfinylphenyl]-1-piperidinyl]butyl]-*N*-methylamine[9] (173 mg, 0.38 mmol), and the resulting mixture was stirred for 2 h. The mixture was partitioned between DCM and water, the layers were separated, the DCM layer was dried ($MgSO_4$) and filtered, and the solvent was removed under reduced pressure to yield a white foam. This was purified by flash chromatography (eluting with 2%, 4%, and 5% methanol/DCM containing 0.1% NH_4OH) to afford the product (0.145 g, 82%) as a white foam: ^{1}H NMR δ 8.77−8.73 (m), 8.16−8.05 (m), 7.85−7.25 (m), 7.02 (d), 6.91−6.86 (m), 6.72 (d), 6.51 (d), 4.19 (t), 3.65−3.58 (m), 3.45−3.22 (m), 3.02−2.28 (m), 2.14−1.42 (m); MS *m/e* 708.3 (M + 1). The material was dissolved in methanol, and 1 equiv of citric acid (39.2 mg, 0.205 mmol) was added. The mixture was concentrated to afford the product as a white powder. Anal. Calcd for $C_{41}H_{39}Cl_2N_3O_2S{\cdot}1.2C_6H_8O_7{\cdot}0.9H_2O$: C, 60.59; H, 5.32; N, 4.40. Found: C, 60.63; H, 5.13; N, 4.48.

***N*-[2-(*S*)-(3,4-Dichlorophenyl)-4-hydroxybutyl]-*N*-methyl-3-cyano-2-methoxy-1-naphthamide (25).** To a solution of 3-cyano-2-methoxy-1-naphthoic acid (5.04 g, 22.2 mmol) in DCM (50 mL) under nitrogen were added dropwise oxalyl chloride (2.32 mL, 26.6 mmol) and a catalytic amount of *N*,*N*′-dimethylformamide. After being stirred for 3 h, the resulting acid chloride solution was concentrated under reduced pressure, then redissolved in DCM, and added dropwise to a cooled (0 °C) solution of *N*-[2-(*S*)-(3,4-dichlorophenyl)-4-hydroxybutyl]-*N*-methylamine[49] (5.51 g, 22.20 mmol) in DCM (200 mL) and 10% aqueous sodium bicarbonate solution (100 mL), and the resulting mixture was stirred overnight at room temperature. The organic phase was separated, washed with water (25 mL) and brine (25 mL), concentrated, and purified by column chromatography to afford the product (9.3 g, 92%) as a tan solid: ^{1}H NMR (DMSO-d_6) δ 8.67−8.58 (m), 8.07−8.00 (m), 7.72−7.65 (m), 7.64−7.43 (m), 7.42−7.34 (m), 7.02−7.01 (m), 6.98−6.87 (d), 6.77−6.74 (d), 6.31−6.28 (d), 4.55−4.52 (t), 4.35−4.34 (t), 4.03−3.92 (m), 3.78−3.72 (m), 3.68 (s), 3.45−3.37 (m), 3.29−2.89 (m), 2.73 (s), 2.59−2.49 (m), 1.91−1.78 (m), 1.58−1.46 (m); MS *m/e* 457 (M + 1).

***N*-[2-(*S*)-(3,4-Dichlorophenyl)-3-carboxypropyl]-*N*-methyl-3-cyano-2-methoxy-1-naphthamide (26).** Pyridinium dichromate[50] (4.5 g, 12.1 mmol) was added to a solution of **25** (1.5 g, 3.3 mmol) in DMF (20 mL), and the resulting mixture was stirred for 4 h. After filtration, dilution with ethyl acetate, and aqueous extraction of the filtrate, the product was purified by flash chromatography (1.3 g, 84%): ^{1}H NMR (DMSO-d_6) δ 12.28 (s), 8.66−8.62 (m), 8.09−7.95 (m), 7.78−7.76 (m), 7.72−

7.56 (m), 7.52−7.45 (m), 7.40−7.30 (m), 7.11−7.10 (d), 7.04 (s), 7.01 (s), 6.87−6.84 (d), 4.53−4.45 (t), 3.94 (s), 3.92 (s), 3.68 (s), 3.44−3.27 (m), 3.11 (s), 3.02 (s), 2.76−2.73 (m), 2.62 (s), 2.55−2.38 (m); MS *m/e* 471 (M + 1).

***N*-[2-(*S*)-(3,4-Dichlorophenyl)-3-aminocarbonylpropyl]-*N*-methyl-3-cyano-2-methoxy-1-naphthamide (8).** To a stirred solution of **26** (0.50 g, 1.06 mmol) and diisopropylethylamine (0.37 mL, 2.12 mmol) in DCM (20 mL) was added tetramethylfluoroformamidinium hexaflurophosphate (0.33 g, 1.27 mmol). After 20 min, ammonium hydroxybenzotriazole[51] (0.28 g, 2.12 mmol) was added. After 30 min, the solution was extracted with saturated sodium bicarbonate, 1 M HCl, water, and brine and then purified by flash chromatography (0.398 g, 80%): ^{1}H NMR (DMSO-d_6) δ 8.64−8.62 (m), 8.08−7.94 (m), 7.78−7.72 (m), 7.70 (s), 7.67 (s), 7.63−7.58 (m), 7.56−7.50 (m), 7.46−7.39 (m), 7.36−7.32 (m), 7.11 (bs); 7.01−6.98 (m), 6.85−6.76 (m), 6.37−6.34 (d), 4.51−4.43 (t), 4.08−3.99 (m), 3.94 (s), 3.91 (s), 3.73−3.71 (m), 3.67 (s), 3.64−3.61 (m), 3.46−3.28 (m), 3.13 (s), 3.11 (s), 3.06 (s), 2.69 (s), 2.62 (s), 2.56−2.44 (m), 2.34−2.27 (m), 2.16−2.11 (m), 2.07 (s); MS *m/e* 470 (M + 1). Anal. Calcd for $C_{24}H_{21}Cl_2N_3O_3{\cdot}0.5H_2O$: C, 60.13; H, 4.62; N, 8.76. Found: C, 60.22; H, 4.77; N, 8.69.

X-ray Experimental Data. Compound 8. This compound was crystallized from methylene chloride: empirical formula, $C_{24}H_{21}Cl_2N_3O_3{\cdot}CH_2Cl_2$; crystal system, monoclinic; space group, $P2_1$; number of molecules per unit cell, 2; lattice parameters, a = 10.432(2) Å, b = 7.0522(4) Å, c = 18.2035(13) Å, β = 90.825(7)°; unit-cell volume, 1339.1(2) Å^3; least-squares structure refinement on F^2 against all data converged at $R_w(F^2)$ = 0.1920; conventional R index $R(F)$ = 0.0689; S (goodness-of-fit on F^2) = 1.036; $x(\sigma(x))$ (Flack absolute structure parameter and its esd) = −0.02(4); expected values for x are 0 (within 3 esd's) for the correct and +1 for the inverted absolute structure. The crystal structure was solved by direct methods; all non-hydrogen atoms appeared in the initial Fourier map except for the methylene chloride molecule, which was identified after some initial cycles of refinement of the compound molecule only followed by reassigning the methylene chloride atoms in the same asymmetric unit. Hydrogen atoms were generated in the course of refinement with idealized geometries relative to neighboring non-hydrogen atoms. Disorder was noted at the methyl from the amide *N*-methyl group and accounted for in refinement, resulting in two sets of hydrogen positions offset by 60° with occupation factors nearly equal, about 0.5. Although the refinement parameters are within acceptable ranges, the moderate results may be attributed to the methylene chloride molecule being rather poorly defined, as seen in Figure 1 by the large thermal ellipsoids, which suggests that methylene chloride molecules were gradually escaping from the crystal lattice over the course of continued exposure to the X-ray beam during data collection.

Acknowledgment. We gratefully acknowledge James Hulsizer for large-scale synthesis efforts, James Hall for detailed NMR analysis, and Margaret Lin for crystallography support.

Supporting Information Available: Crystallographic data for **8**. This material is available free of charge via the Internet at http://pubs.acs.org.

References

(1) Stout, S. C.; Owens, M. J.; Nemeroff, C. B. Neurokinin-1 receptor antagonists as potential antidepressants. *Annu. Rev. Pharmacol. Toxicol.* **2001**, *41*, 877−906.
(2) Chahl, L. A.; Urban, L. A. New developments in tachykinin research. *Pharmacol. Rev. Commun.* **1999**, *10*, 197−203.
(3) Swain, C.; Rupniak, N. M. J. Progress in the development of neurokinin antagonists. *Annu. Rep. Med. Chem.* **1999**, *34*, 51−60.
(4) Gerspacher, M.; Von Sprecher, A. Dual neurokinin NK_1/NK_2 receptor antagonists. *Drugs Future* **1999**, *24*, 883−892.
(5) Gao, Z.; Peet, N. P. Recent advances in neurokinin receptor antagonists. *Curr. Med. Chem.* **1999**, *6*, 375−388.
(6) Sakurada, T.; Sakurada, C.; Tan-No, K.; Kisara, K. Neurokinin receptor antagonists: therapeutic potential in the treatment of pain syndromes. *CNS Drugs* **1997**, *8*, 436−447.
(7) Bernstein, P. R.; Aharony, D.; Albert, J. S.; Andisik, D.; Barthlow, H. G.; Bialecki, R.; Davenport, T.; Dedinas, R. F.; Dembofsky, B. T.; Koether, G.; Kosmider, B. J.; Kirkland, K.; Ohnmacht, C. J.; Potts, W.; Rumsey, W. L.; Shen, L.; Shenvi, A.; Sherwood, S.; Stollman, D.; Russell, K. Discovery of novel, orally active dual NK_1/NK_2 antagonists. *Bioorg. Med. Chem. Lett.* **2001**, *11*, 2769−2773.
(8) Rumsey, W. L.; Aharony, D.; Bialecki, R. A.; Abbott, B. M.; Barthlow, H. G.; Caccese, R.; Ghanekar, S.; Lengel, D.; McCarthy, M.; Wenrich, B.; Undem, B.; Ohnmacht, C.; Shenvi, A.; Albert, J. S.; Brown, F.; Bernstein, P. R.; Russell, K. Pharmacological characterization of ZD6021: a novel, orally active antagonist of the tachykinin receptors. *J. Pharmacol. Exp. Ther.* **2001**, *298*, 307−315.
(9) Albert, J. S.; Aharony, D.; Andisik, D.; Barthlow, H.; Bernstein, P. R.; Bialecki, R. A.; Dedinas, R.; Dembofsky, B. T.; Hill, D.; Kirkland, K.; Koether, G. M.; Kosmider, B. J.; Ohnmacht, C.; Palmer, W.; Potts, W.; Rumsey, W.; Shen, L.; Shenvi, A.; Sherwood, S.; Warwick, P. J.; Russell, K. Design, synthesis, and SAR of tachykinin antagonists: Modulation of balance in NK1/NK2 receptor antagonist activity. *J. Med. Chem.* **2002**, *45*, 3972−3983.
(10) Testa, B.; Carrupt, P.-A.; Gal, J. The so-called "interconversion" of stereoisomeric drugs: an attempt at clarification. *Chirality* **1993**, *5*, 105−111.
(11) Friary, R. J.; Spangler, M.; Osterman, R.; Schulman, L.; Schwerdt, J. H. Enantiomerization of an atropisomeric drug. *Chirality* **1996**, *8*, 364−371.
(12) Hauser, F. M.; Sengupta, D.; Corlett, S. A. Optically active total synthesis of Calphostin D. *J. Org. Chem.* **1994**, *59*, 1967−1969.
(13) Oki, M. *The Chemistry of Rotatonal Isomers*; Springer-Verlag: New York, 1993.
(14) Ahmed, A.; Bragg, R. A.; Clayden, J.; Lai, L. W.; McCarthy, C.; Pink, J. H.; Westlund, N.; Yasin, S. A. Barriers to rotation about the chiral axis of tertiary aromatic amides. *Tetrahedron* **1998**, *54*, 13277−13294.
(15) Clayden, J.; McCarthy, C.; Helliwell, M. Bonded peri-interactions govern the rate of racemization of atropisomeric 8-substituted 1-naphthamides. *Chem. Commun.* **1999**, 2059−2060.
(16) Clayden, J.; Pink, J. H. Concerted rotation in a tertiary aromatic amide: towards a simple molecular gear. *Angew. Chem., Int. Ed.* **1998**, *37*, 1937−1939.
(17) For compounds that displayed nonpurely competitive antagonism, activity could be estimated by monitoring the magnitude of the maximum tissue relaxation response (percent of control response) to increasing agonist concentration following incubation of the tissue with the antagonist at a given concentration. Values are expressed as percent inhibition, which is calculated by (100 − percentage of control response). Thus, greater antagonist potency would be indicated by greater percent inhibition and at lower antagonist concentration.
(18) Rupniak, N. M. J.; Tattersall, F. D.; Williams, A. R.; Rycroft, W.; Carlson, E. J.; Cascieri, M. A.; Sadowski, S.; Ber, E.; Hale, J. J.; Mills, S. G.; MacCoss, M.; Seward, E.; Huscroft, I.; Owen, S.; Swain, C. J.; Hill, R. G.; Hargreaves, R. J. In vitro and in vivo predictors of the anti-emetic activity of tachykinin NK1 receptor antagonists. *Eur. J. Pharmacol.* **1997**, *326*, 201−209.
(19) Iwamura, H.; Mislow, K. Stereochemical consequences of dynamic gearing. *Acc. Chem. Res.* **1988**, *21*, 175−182.
(20) Manuscript in preparation.
(21) Swain, C. J.; Sewart, E. M.; Cascieri, M. A.; Fong, T. M.; Herbert, R.; MacIntyre, D. E.; Merchant, K. J.; Owen, S. N.; Owens, A. P.; et al. Identification of a series of 3-(benzyloxy)-1-azabicyclo-[2.2.2]octane human NK1 antagonists. *J. Med. Chem.* **1995**, *38*, 4793−4805.
(22) Lowe, J. A., III; Drozda, S. E.; Snider, R. M.; Longo, K. P.; Zorn, S. H.; Morrone, J.; Jackson, E. R.; McLean, S.; Bryce, D. K.; et al. The discovery of (2S,3S)-*cis*-2-(diphenylmethyl)-N-[(2-methoxyphenyl)methyl]-1-azabicyclo[2.2.2]octan-3-amine as a novel, nonpeptide substance P antagonist. *J. Med. Chem.* **1992**, *35*, 2591−2600.
(23) Boks, G. J.; Tollenaere, J. P.; Kroon, J. Possible ligand−receptor interactions for NK1 antagonists as observed in their crystal structures. *Bioorg. Med. Chem.* **1997**, *5*, 535−547.
(24) Caliendo, G.; Grieco, P.; Perissutti, E.; Santagada, V.; Saviano, G.; Tancredi, T.; Temussi, P. A. Conformational analysis of three NK1 tripeptide antagonists: A proton nuclear magnetic resonance study. *J. Med. Chem.* **1997**, *40*, 594−601.
(25) Veenstra, S. J.; Hauser, K.; Betschart, C. Studies on the active conformation of NK1 antagonist CGP 49823. Part 1. Synthesis of conformationally restricted analogs. *Bioorg. Med. Chem. Lett.* **1997**, *7*, 347−350.
(26) Desai, M. C.; Lefkowitz, S. L.; Thadeio, P. F.; Longo, K. P.; Snider, R. M. Discovery of a potent substance P antagonist: recognition of the key molecular determinant. *J. Med. Chem.* **1992**, *35*, 4911−4913.

(27) Stevenson, G. I.; Huscroft, I.; MacLeod, A. M.; Swain, C. J.; Cascieri, M. A.; Chicchi, G. G.; Graham, M. I.; Harrison, T.; Kelleher, F. J.; Kurtz, M.; Ladduwahetty, T.; Merchant, K. J.; Metzger, J. M.; MacIntyre, D. E.; Sadowski, S.; Sohal, B.; Owens, A. P. 4,4-Disubstituted piperidine high-affinity NK1 antagonists: Structure−activity relationships and in vivo activity. *J. Med. Chem.* **1998**, *41*, 4623−4635.

(28) Lewis, R. T.; Macleod, A. M.; Merchant, K. J.; Kelleher, F.; Sanderson, I.; Herbert, R. H.; Cascieri, M. A.; Sadowski, S.; Ball, R. G.; Hoogsteen, K. Tryptophan-derived NK1 antagonists: Conformationally constrained heterocyclic bioisosteres of the ester linkage. *J. Med. Chem.* **1995**, *38*, 923−933.

(29) Ikeura, Y.; Ishichi, Y.; Tanaka, T.; Fujishima, A.; Murabayashi, M.; Kawada, M.; Ishimaru, T.; Kamo, I.; Doi, T.; Natsugari, H. Axially chiral N-benzyl-N,7-dimethyl-5-phenyl-1,7-naphthyridine-6-carboxamide derivatives as tachykinin NK1 receptor antagonists: Determination of the absolute stereochemical requirements. *J. Med. Chem.* **1998**, *41*, 4232−4239.

(30) Sisto, A.; Bonelli, F.; Centini, F.; Fincham, C. I.; Potier, E.; Monteagudo, E.; Lombardi, P.; Arcamone, F.; Goso, C.; et al. Synthesis and biological evaluation of novel NK-1 tachykinin receptor antagonists: the use of cycloalkyl amino acids as a template. *Biopolymers* **1995**, *36*, 511−524.

(31) Greenfeder, S.; Cheewatrakoolpong, B.; Anthes, J.; Billah, M.; Egan, R. W.; Brown, J. E.; Murgolo, N. J. Two related neurokinin-1 receptor antagonists have overlapping but different binding sites. *Bioorg. Med. Chem.* **1998**, *6*, 189−194.

(32) Jacoby, E.; Boudon, A.; Kucharczyk, N.; Michel, A.; Fauchere, J.-L. A structural rationale for the design of water soluble peptide-derived neurokinin-1 antagonists. *J. Recept. Signal Transduction Res.* **1997**, *17*, 855−873.

(33) Takeuchi, Y.; Shands, E. F. B.; Beusen, D. D.; Marshall, G. R. Derivation of a 3-dimensional pharmacophore model of substance P antagonists bound to the neurokinin-1 receptor. *J. Med. Chem.* **1998**, *41*, 3609−3623.

(34) Hale, J. J.; Mills, S. G.; MacCoss, M.; Finke, P. E.; Cascieri, M. A.; Sadowski, S.; Ber, E.; Chicchi, G. G.; Kurtz, M.; Metzger, J.; Eiermann, G.; Tsou, N. N.; Tattersall, F. D.; Rupniak, N. M. J.; Williams, A. R.; Rycroft, W.; Hargreaves, R.; MacIntyre, D. E. Structural optimization affording 2-(R)-(1-(R)-3,5-bis(trifluoromethyl)phenylethoxy)-3-(S)-(4-fluoro)phenyl-4-(3-oxo-1,2,4-triazol-5-yl)methylmorpholine, a potent, orally active, long-acting morpholine acetal human NK-1 receptor antagonist. *J. Med. Chem.* **1998**, *41*, 4607−4614.

(35) Kramer, M. S.; Cutler, N.; Feighner, J.; Shrivastava, R.; Carman, J.; Sramek, J. J.; Reines, S. A.; Liu, G.; Snavely, D.; Wyatt-Knowles, E.; Hale, J. J.; Mills, S. G.; MacCoss, M.; Swain, C. J.; Harrison, T.; Hill, R. G.; Hefti, F.; Scolnick, E. M.; Cascieri, M. A.; Chicchi, G. G.; Sadowski, S.; Williams, A. R.; Hewson, L.; Smith, D.; Carlson, E. J.; Hargreaves, R. J.; Rupniak, N. M. J. Distinct mechanism for antidepressant activity by blockade of central substance P receptors. *Science (Washington, D.C.)* **1998**, *281*, 1640−1645.

(36) Seward, E. M.; Carlson, E.; Harrison, T.; Haworth, K. E.; Herbert, R.; Kelleher, F. J.; Kurtz, M. M.; Moseley, J.; Owen, S. N.; Owens, A. P.; Sadowski, S. J.; Swain, C. J.; Williams, B. J. Spirocyclic NK1 antagonists I: [4.5] and [5.5]-spiroketals. *Bioorg. Med. Chem. Lett.* **2002**, *12*, 2515−2518.

(37) *CATALYST*, version 4.5; Molecular Simulations Inc.: San Diego, CA.

(38) Aharony, D.; Little, J.; Thomas, C.; Powell, S.; Berry, D.; Graham, A. Isolation and pharmacological characterization of a hamster urinary bladder neurokinin A receptor cDNA. *Mol. Pharmacol.* **1994**, *45*, 9−19.

(39) Graham, A.; Hopkins, B.; Powell, S. J.; Danks, P.; Briggs, I. Isolation and characterization of the human lung NK-2 receptor gene using rapid amplification of cDNA ends. *Biochem. Biophys. Res. Commun.* **1991**, *177*, 8−16.

(40) Huang, R.; Cheung, A.; Mazina, K.; Strader, C.; Fong, T. cDNA Sequence and heterologous expression of the human neurokinin-3 receptor. *Biochem. Biophys. Res. Commun.* **1992**, *184*, 966−972.

(41) Takeda, Y.; Chou, K. B.; Takeda, J.; Sachais, B. S.; Krause, J. E. Molecular cloning, structural characterization and functional expression of the human substance P receptor. *Biochem. Biophys. Res. Commun.* **1991**, *179*, 1232−1240.

(42) Fong, T. M.; Anderson, S. A.; Yu, H.; Huang, R. R. C.; Strader, C. D. Differential activation of intracellular effector by two isoforms of human neurokinin-1 receptor. *Mol. Pharmacol.* **1992**, *41*, 24−30.

(43) Gerard, N. P.; Garraway, L. A.; Eddy, R. L., Jr.; Shows, T. B.; Iijima, H.; Paquet, J. L.; Gerard, C. Human substance P receptor (NK-1): organization of the gene, chromosome localization and functional expression of cDNA clones. *Biochemistry* **1991**, *30*, 10640−10646.

(44) Takahashi, K.; Tanaka, A.; Hara, M.; Nakanishi, S. The primary structure and gene organization of human substance P and neuromedin K receptors. *Eur. J. Biochem.* **1992**, *204*, 1025−1033.

(45) Buell, G.; Schulz, M. F.; Arkinstall, S. J.; Maury, K.; Missotten, M.; Adami, N.; Talabot, F.; Kawashima, E. Molecular characterization, expression and localization of human neurokinin-3 receptor. *FEBS Lett.* **1992**, *299*, 90−95.

(46) Aharony, D.; Buckner, C. K.; Ellis, J. L.; Ghanekar, S. V.; Graham, A.; Kays, J. S.; Little, J.; Meeker, S.; Miller, S. C.; et al. Pharmacological characterization of a new class of nonpeptide neurokinin A antagonists that demonstrate species selectivity. *J. Pharmacol. Exp. Ther.* **1995**, *274*, 1216−1221.

(47) AESOP is an in-house molecular mechanics program (Masek, B.) derived from BIGSTRN-3 (QCPE-514): Nachbar, R., Jr.; Mislow, K. *QCPE Bull.* **1986**, *6*, 96.

(48) ENIGMA is an in-house molecular graphics program.

(49) Miller, S. C. (Zeneca Ltd., U.K.). Novel 4-piperidinyl-substituted lactams as neurokinin 2 receptor antagonists for the treatment of asthma. PCT Int. Appl. WO 9512577, 1995.

(50) Corey, E. J.; Schmidt, G. Useful procedures for the oxidation of alcohols involving pyridinium dichromate in aprotic media. *Tetrahedron Lett.* **1979**, 399−402.

(51) Bajusz, S.; Ronai, A. Z.; Szekely, J. I.; Graf, L.; Dunai-Kovacs, Z.; Berzetei, I. A superactive antinociceptive pentapeptide, (D-Met2, Pro5)-enkephalinamide. *FEBS Lett.* **1977**, *76*, 91−92.

JM030197G